

Cramér Rao Bound Analysis for Cooperative Positioning in Intelligent Transportation Systems

Jelena Gabela

University of Melbourne, Melbourne, Australia
jgabela@student.unimelb.edu.au

Salil Goel

RMIT University, Melbourne, Australia
salil.goel@rmit.edu.au

Allison Kealy

RMIT University, Melbourne, Australia
allison.kealy@rmit.edu.au

Mark Hedley

CSIRO Data61, Australia
Mark.Hedley@data61.csiro.au

Bill Moran

University of Melbourne, Melbourne, Australia
wmoran@unimelb.edu.au

Simon Williams

RMIT University, Melbourne, Australia
simon.williams@rmit.edu.au

ABSTRACT

With the development of Intelligent Transport Systems (ITS), requirements for better integrity, accuracy, and availability are becoming important due to the increasing safety implications of these systems. Thus, development of a positioning solution that satisfies ITS requirements has been a relevant challenge for years. The past decade has witnessed the development of ITS with an emphasis on sensor integration. In recent years, a significant amount of work has been done in the domain of cooperative positioning where it has been demonstrated that sharing of information between nodes in a network is beneficial, especially in GNSS denied environments. An ITS cooperative positioning system comprises multiple dynamic nodes (e.g. cars) and static nodes (e.g. infrastructure), each of which is equipped with multiple sensors for positioning and relative range measurements. In cooperative positioning, nodes assist each other in positioning by sharing information about themselves and relative information with respect to neighbouring nodes. Posterior Cramér Rao Bounds (PCRB) is a standard method for evaluating the best theoretical performance of a positioning system. This paper derives the PCRB for cooperative positioning in a dynamic ITS and demonstrates the use of the

derived bounds for analysing the system performance with respect to different network parameters. The performance of Vehicle-to-Infrastructure, Vehicle-to-Vehicle and combined cooperative positioning for an ad-hoc network of four vehicles and 15 infrastructure nodes is assessed. It is shown that the number of available infrastructure nodes and their geometry can significantly affect the performance. The analysis presented in this paper can be used for designing and developing a robust ITS.

KEYWORDS: Cooperative positioning, GNSS, Intelligent Transport Systems, Posterior Cramér Rao Bounds.

1. INTRODUCTION

As Intelligent Transport Systems (ITS) are deployed and their accuracy, integrity and availability requirements are becoming more stringent, increasing the need for positioning solution that satisfies those requirement. This poses an increasing challenge, especially in urban environments, as current positioning solutions rely on Global Navigation Satellite Systems (GNSS). The majority of today's positioning solutions are based on sensor integration, where integration of GNSS and Inertial Measurements Units (IMU) is most often proposed. Although this integration assures positioning solution availability, it does not assure reliability nor accuracy, which are very important in ITS safety-critical and liability-critical applications (e.g. anti-collision systems and toll charging). The main problem of GNSS/IMU integration is that the accuracy of positioning solution depends on having a precise GNSS available in order to reinitialise IMU measurements and prevent the solution from drifting due to the accumulation of errors in the IMU. This can become a big problem for ITS in urban environments, where loss of GNSS over a long period of time can cause significant degradation of accuracy. Therefore, in recent years, a lot of work has been done in the domain of cooperative positioning (CP). CP techniques utilise sharing of measurement information between static or dynamic nodes in an ITS network (i.e. vehicles, infrastructure) in order to improve positioning system's overall performance (Alam and Dempster, 2013). This approach has proven to be beneficial for positioning systems' performance (Goel *et al.*, 2016; Goel, 2017; Goel *et al.*, 2017; Yao *et al.*, 2011). Posterior Cramér Rao Bounds (PCRB) can provide information about the theoretically best achievable performance of any positioning system based on the ground truth. This is a valuable information when it comes to assessing the adequacy of used estimators.

This paper demonstrates benefits of CP in ad-hoc network of four vehicles and 15 infrastructure nodes, where one vehicle does not have GNSS information for the entire duration of the simulation. The performance of Vehicle-to-Infrastructure (V-2-I), Vehicle-to-Vehicle (V-2-V), and V-2-I + V-2-V CP is assessed using PCRB and position estimation accuracy. PCRB is used to assess the performance of the developed CP system and analyse the effect of various parameters such as network geometry on the overall performance. For a solution to be appropriate for ITS, it should show the accuracy and PCRB better than 0.5 m (Shladover and Tan, 2006; Alam and Dempster, 2013), which assures lane-level positioning as a starting point for any ITS application.

The Sections 2 and 3 present a brief overview of the related work followed by the details of a centralised cooperative positioning framework. The framework is generalised and it can be applied for any number of mobile or infrastructure nodes. Full definition of parameters used in this particular simulation can be found in following sections. Section 4 presents the details of simulations of ad-hoc vehicle and infrastructure network. The results of the developed system including V2I, V2V and V2I + V2V cooperative positioning are presented and analysed in

Section 5. Lastly, Section 6 presents the conclusions of this paper and provides suggestions for the future work.

2. BACKGROUND OF POSTERIOR CRAMÉR RAO BOUND

Posterior Cramér Rao Bound (PCRB) can be used to find the best theoretically achievable performance of CP. Although Gholami *et al.* (2012), Larsson (2004) and Penna *et al.* (2010) derive expressions for CRB CP, they are derived for static CP systems and therefore cannot be used for proposed dynamic CP system.

The expression for PCRB used in this paper was firstly derived by Taylor (1979). In order to derive the PCRB for a dynamic nonlinear positioning system, an estimator needs to be used. Taylor (1979) has shown that Fisher information matrix “propagates according to the same equations as the filter covariance matrix for an Extended Kalman Filter (EKF) linearized about the true (unknown) trajectory”. Thus, an EKF is used as the estimator in this paper. It is important to note that, based on Taylor’s definition of PCRB, it can only be assessed for the trajectories where the ground truth is known (i.e. simulations). Therefore, it is a useful tool to estimate if the EKF or any other estimator is adequate for the proposed nonlinear dynamic system and if the effort should be put in developing an appropriate mathematical model. Although Taylor’s expression for PCRB has been derived without assuming process noise, it has been shown in Popescu *et al.* (2013) that process noise can simply be added to one of the summands in Taylor’s original expression. Consequently, propagation of the posterior Fisher information matrix and PCRB matrix is given as:

$$J_{k+1} = (F_k J_k F_k^T + Q_k)^{-1} + H_{k+1}^T R_{k+1}^{-1} H_{k+1} \quad (1)$$

$$PCRB = J_{k+1}^{-1} \quad (2)$$

where F_k denotes state transition matrix, J_k denotes Fisher information matrix for time instant k , Q_k denotes process noise, H_{k+1} denotes measurement matrix, and R_{k+1} denotes measurement noise. Notion $(\cdot)^T$ is used to denote transpose matrix. The PCRB is then calculated by finding an inverse to the Fisher information matrix.

3. CENTRALISED COOPERATIVE POSITIONING FRAMEWORK

A network of N_m mobile nodes (i.e. vehicles) and N_i infrastructure nodes is considered. It is assumed that positions of infrastructure nodes have been precisely determined in a global coordinate reference system. Positions of N_a mobile nodes are known and they have been determined at every time instant using GNSS. $N_u = N_m - N_a$ mobile nodes are assumed not to have access to GNSS signal. In order to determine positions of N_u mobile nodes, other mobile nodes cooperatively share their positions and relative ranges between each N_u and N_a . It is to be noted that relative ranges between all mobile nodes are measured with methods such as Ultra-WideBand (UWB), which enables V-2-V CP. Furthermore, it is assumed that relative ranges between all N_u mobile nodes and N_i infrastructure nodes are measured as well. This enables V-2-I CP.

A mathematical model for the EKF used in this paper is a variation of the model developed in

Goel *et al.* (2016). There, a detailed mathematical model for centralised and distributed cooperative positioning can be found. The authors in Goel *et al.* (2016) and Goel *et al.* (2017) have demonstrated the benefits of CP and have demonstrated their mathematical frameworks on the example of Unmanned Aerial Vehicles (UAVs). This paper extends their mathematical model for centralised CP and demonstrates its performance for ITS applications.

In a centralised CP system, the joint state vector is given as:

$$X = \begin{bmatrix} (x_1)^T & \cdots & (x_{N_u})^T & (x_{N_{u+1}})^T & \cdots & (x_{N_m})^T \end{bmatrix}^T \quad (3)$$

where x_i denotes a state vector for the i^{th} mobile node and it is defined in the equation below. N_u denotes the last mobile node with unavailable GNSS trajectory, N_{u+1} denotes the first mobile node with a known GNSS trajectory, and N_m denotes the last mobile node in general as well as the last node with known GNSS trajectory.

$$x_i = \begin{bmatrix} (r_i)^T & (v_i)^T \end{bmatrix}^T \quad (4)$$

The state vector x_i for single node consists of six states where r_i denotes 3D position estimate, and v_i denotes 3D velocity estimate. The evolution of joint state vector can be expressed as follows.

$$\dot{X} = f(X) \quad (5)$$

$$X_{k+1} = X_k + f(X_k)\delta t \quad (6)$$

Where equation 5 represents a general expression and equation 6 represents the evolution of state vector used in this paper. In this particular simulation, constant velocity of the vehicles was used, however this model is not constant velocity model. In that case, the state transition matrix for a single mobile node and for all nodes respectively can be defined as:

$$F_{k+1}^i = \begin{bmatrix} I_{3 \times 3} & I \cdot \delta t \\ 0 & I_{3 \times 3} \end{bmatrix} \quad (7)$$

$$F_{k+1} = \begin{bmatrix} F_{k+1}^1 & \cdots & 0 & 0 & \cdots & 0 \\ \vdots & \ddots & \vdots & \vdots & \vdots & \vdots \\ 0 & \cdots & F_{k+1}^{N_u} & 0 & \cdots & 0 \\ 0 & \cdots & 0 & F_{k+1}^{N_{u+1}} & \cdots & 0 \\ \vdots & \vdots & \vdots & \vdots & \ddots & \vdots \\ 0 & \cdots & 0 & 0 & \cdots & F_{k+1}^{N_m} \end{bmatrix}_{N_m \times N_m} \quad (8)$$

where δt denotes time increment between states $(k+1)$ and k , and I denotes an identity matrix. As stated before, in this framework, all mobile nodes are communicating (i.e. sharing relative ranges) among themselves, and all mobile nodes with unavailable GNSS measurements are communicating with infrastructure nodes. Additionally, all mobile nodes with available GNSS measurements are sharing their GNSS positions. This paper uses a loosely coupled EKF

for numerical simulations, i.e. the presence of position measurements from GNSS instead of pseudoranges is assumed. Thus, a measurement vector Z_{k+1} for time instant $(k+1)$ can be defined as:

$$Z_{k+1} = \begin{bmatrix} (d_{u,a})^T & (d_{a,a})^T & (d_{u,i})^T & (r_a^{GNSS})^T \end{bmatrix}^T \quad (9)$$

where $d_{u,a}$ denotes all ranges measured between mobile nodes with unavailable and available GNSS measurements, $d_{a,a}$ denotes all ranges measured between mobile nodes with available GNSS measurements, and $d_{u,i}$ denotes all the ranges measured between mobile nodes with unavailable GNSS measurements and infrastructure nodes. Since ranges between mobile nodes with available GNSS measurements and infrastructure nodes are not measured, $d_{a,i}$ vector is not the part of the measurement vector, although it can certainly be added. Available GNSS positions are denoted with r_a^{GNSS} . With that in mind, the measurement matrix for the overall network can be obtained by linearising measurement equations with respect to the nodes involved. The measurement model for relative ranges between any two nodes i and j is given as:

$$d_{i,j} = \sqrt{(x_i - x_j)^2 + (y_i - y_j)^2 + (z_i - z_j)^2} + e_{d_{ij}} \quad (10)$$

where $d_{i,j}$ denotes the distance between predicted positions of nodes $X_i(x_i, y_i, z_i)$ and $X_j(x_j, y_j, z_j)$. The measurement matrix H_{k+1} can be written as follows,

$$H_{k+1} = \begin{bmatrix} H_{k+1}^{d_{1,2}^1} & H_{k+1}^{d_{1,2}^2} & H_{k+1}^{d_{1,2}^3} & \dots & H_{k+1}^{d_{1,2}^{(N_u+1)}} & \dots & H_{k+1}^{d_{1,2}^{N_m}} \\ \vdots & \vdots & \vdots & \dots & \vdots & \dots & \vdots \\ H_{k+1}^{d_{Nu,Nm}^1} & H_{k+1}^{d_{Nu,Nm}^2} & H_{k+1}^{d_{Nu,Nm}^3} & \dots & H_{k+1}^{d_{Nu,Nm}^{(N_u+1)}} & \dots & H_{k+1}^{d_{Nu,Nm}^{N_m}} \\ H_{k+1}^{d_{Nu+1,Nu+2}^1} & H_{k+1}^{d_{Nu+1,Nu+2}^2} & H_{k+1}^{d_{Nu+1,Nu+2}^3} & \dots & H_{k+1}^{d_{Nu+1,Nu+2}^{(N_u+1)}} & \dots & H_{k+1}^{d_{Nu+1,Nu+2}^{N_m}} \\ \vdots & \vdots & \vdots & \dots & \vdots & \dots & \vdots \\ H_{k+1}^{d_{Nm-1,Nm}^1} & H_{k+1}^{d_{Nm-1,Nm}^2} & H_{k+1}^{d_{Nm-1,Nm}^3} & \dots & H_{k+1}^{d_{Nm-1,Nm}^{(N_u+1)}} & \dots & H_{k+1}^{d_{Nm-1,Nm}^{N_m}} \\ H_{k+1}^{d_{1,a}^1} & H_{k+1}^{d_{1,a}^2} & H_{k+1}^{d_{1,a}^3} & \dots & H_{k+1}^{d_{1,a}^{(N_u+1)}} & \dots & H_{k+1}^{d_{1,a}^{N_m}} \\ \vdots & \vdots & \vdots & \dots & \vdots & \dots & \vdots \\ H_{k+1}^{d_{1,Ni}^1} & H_{k+1}^{d_{1,Ni}^2} & H_{k+1}^{d_{1,Ni}^3} & \dots & H_{k+1}^{d_{1,Ni}^{(N_u+1)}} & \dots & H_{k+1}^{d_{1,Ni}^{N_m}} \\ H_{k+1}^{d_{2,a}^1} & H_{k+1}^{d_{2,a}^2} & H_{k+1}^{d_{2,a}^3} & \dots & H_{k+1}^{d_{2,a}^{(N_u+1)}} & \dots & H_{k+1}^{d_{2,a}^{N_m}} \\ \vdots & \vdots & \vdots & \dots & \vdots & \dots & \vdots \\ H_{k+1}^{d_{2,Ni}^1} & H_{k+1}^{d_{2,Ni}^2} & H_{k+1}^{d_{2,Ni}^3} & \dots & H_{k+1}^{d_{2,Ni}^{(N_u+1)}} & \dots & H_{k+1}^{d_{2,Ni}^{N_m}} \\ H_{k+1}^{d_{Nu,a}^1} & H_{k+1}^{d_{Nu,a}^2} & H_{k+1}^{d_{Nu,a}^3} & \dots & H_{k+1}^{d_{Nu,a}^{(N_u+1)}} & \dots & H_{k+1}^{d_{Nu,a}^{N_m}} \\ \vdots & \vdots & \vdots & \dots & \vdots & \dots & \vdots \\ H_{k+1}^{d_{Nu,Ni}^1} & H_{k+1}^{d_{Nu,Ni}^2} & H_{k+1}^{d_{Nu,Ni}^3} & \dots & H_{k+1}^{d_{Nu,Ni}^{(N_u+1)}} & \dots & H_{k+1}^{d_{Nu,Ni}^{N_m}} \\ 0_{3 \times 6} & 0_{3 \times 6} & 0_{3 \times 6} & \dots & I_{3 \times 3} | 0_{3 \times 3} & \dots & 0_{3 \times 6} \\ \vdots & \vdots & \vdots & \dots & \vdots & \dots & \vdots \\ 0_{3 \times 6} & 0_{3 \times 6} & 0_{3 \times 6} & \dots & 0_{3 \times 6} & \dots & I_{3 \times 3} | 0_{3 \times 3} \end{bmatrix} \quad (11)$$

where $H_{k+1}^{d_i j}$ denotes the Jacobian matrix for the distance d_i in respect to the node j and is given as follows.

$$H_{k+1}^{d_i j} = \begin{bmatrix} \frac{\partial d_i}{\partial x_j} & \frac{\partial d_i}{\partial y_j} & \frac{\partial d_i}{\partial z_j} & 0 & 0 & 0 \end{bmatrix} \quad (12)$$

It is to be noted that, many of these matrices are going to be equal to zero because the Jacobian of the distance d_i with respect to node j is going to be zero. Furthermore, the joint measurement matrix has a similar structure to the measurement vector from equation 10. Firstly, Jacobian matrices for distances between mobile nodes that have unavailable and available GNSS are calculated. Then, Jacobian matrices for distances between mobile nodes that have GNSS available are derived which is followed by the Jacobian matrices for distances between mobile nodes that cannot receive GNSS signal and infrastructure nodes. Then, Jacobian matrices for GNSS positions are derived. Since the EKF is loosely-coupled, Jacobians of a certain coordinate of the mobile node with available GNSS is going to be equal to the identity matrix.

Having defined the transition matrix and the measurement matrix, and with the assumptions that the process noise w_{k+1} and observation noise v_{k+1} are additive white and Gaussian, (i.e. $w_{k+1} \sim N(0, Q_k)$ and $v_{k+1} \sim N(0, R_k)$), the standard EKF equations can be used for estimating the trajectory.

The next section explains the simulation setup and simulated measurements in cooperative ITS. Based on the described simulation, if H_{k+1} is determined by linearising measurement model about the true trajectory instead of predicted one, as stated in Taylor (1979), then that matrix can be used to calculate PCRB.

4. AD-HOC VEHICLE AND INFRASTRUCTURE NETWORK DATA SIMULATION

In order to test the performance of the proposed dynamic centralised CP framework on cars, a network of four cars and 15 infrastructure nodes is used. This paper assumes that all cars are able to communicate amongst themselves. In addition, the car without GNSS can communicate with static infrastructure nodes. It is assumed, that the cars are using Continuously Operating Reference Station (CORS) Real Time Kinematic (RTK) GNSS which provides a solution with an accuracy of 2 cm in 2D and 4 cm in heights. Relative ranges are assumed to be measured with Ultra-WideBand (UWB) radios, which are expected to dynamically measure relative ranges between any two cars or between a car and infrastructure nodes with an accuracy of 1 m. The simulated road is assumed to be 10.5 m wide and the positions of infrastructure nodes are simulated to follow the road network with approximate relative distances of 19 m.

Cars are moving in a loop along the road with a constant velocity of 5 m/s on the straight parts of trajectory and 1 rad/s in turns, for approximately 5 min. It is assumed that Car 1 cannot receive GNSS measurements. Its trajectory is more complicated than for the other cars because Car 1 turns right into the small loop at some point (Figure 1). Car 2 follows Car 1 until Car 1 turns, where Car 2 continues driving on the normal trajectory (Figure 2). Car 3 and 4 are starting from the east side of the road and are driving in the opposite direction from Car 1 and 2, constantly following each other (Figure 3 and 4). The red arrow marks the starting point of each car in Figures 1 to 4. Based on these trajectories, synthetic measurements are generated. As mentioned before, measurement errors are assumed to follow Gaussian distribution with 2 cm

standard deviation of 2D GNSS, 4 cm standard deviation of GNSS heights, and 1 m standard deviation in relative range measurements. Furthermore, inverse of the initial state covariance matrix has been used as the initial Fisher information matrix. Moreover, different process noise is used for straight parts of the trajectory and turns because of different dynamics of driving straight and turning. It is assumed that the data rate is 50 Hz, i.e. measurements are available at every 0.02 seconds. The next section presents the results and analyses the performance of this system.

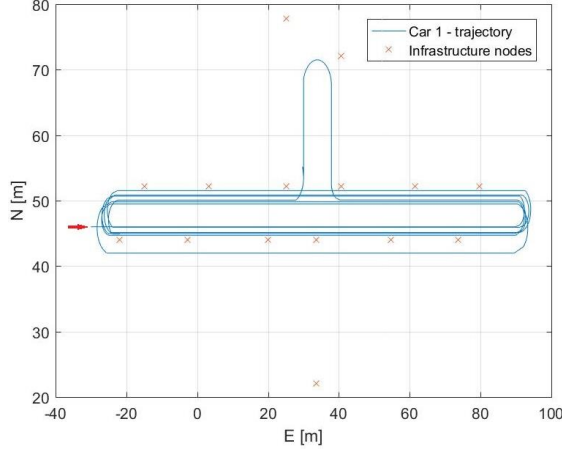


Figure 1. Simulated trajectory of Car 1

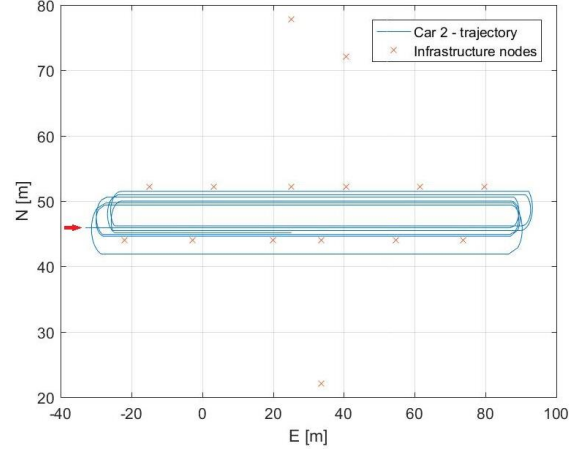


Figure 2. Simulated trajectory of Car 2

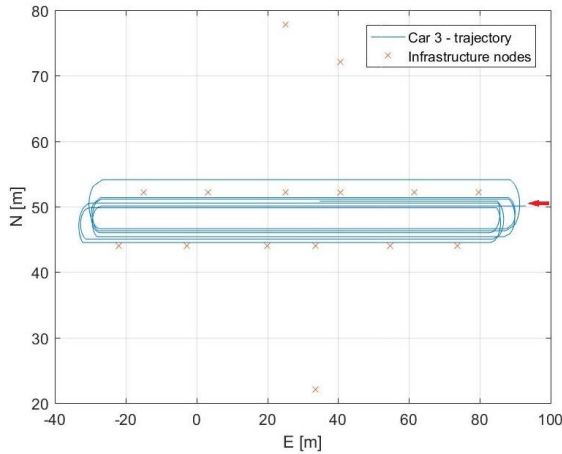


Figure 3. Simulated trajectory of Car 3

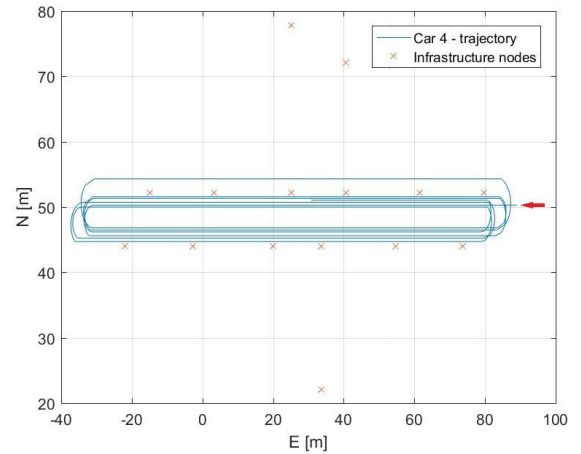


Figure 4. Simulated trajectory of Car 4

5. RESULTS AND DISCUSSION

This section is divided into 3 subsection, where each presents a different approach to CP. In the first subsection, the performance of V-2-I CP is assessed and analysed. The second subsection, briefly introduces the V-2-V cooperative and the last one assesses the performance of combined V-2-I and V-2-V CP performance.

5.1 Vehicle to Infrastructure Cooperative Positioning

In these experiments, it is assumed that Car 1 does not have any GNSS measurements. Instead, it estimates its own position based solely on the relative range measurements to all available infrastructure nodes (V-2-I). The mathematical model presented in Section 3 can be adapted for this case simply by including only ranges measured to infrastructure nodes in the measurement

vector Z_{k+1} , and by adapting joint measurement matrix H_{k+1} accordingly.

The performance of V-2-I is tested based on the different geometries and number of infrastructure nodes. Principal performance metrics are PCRB and accuracy. Firstly, the performance of CP for the network of 15 infrastructure nodes is tested. Figure 5 shows the estimated trajectory of the Car 1 when relative ranges to 15 nodes are measured. Estimated trajectory seems to be well estimated, except in cases when the car transitions from a straight trajectory to turns. In this paper, different process noise is used for straight parts of the trajectory and turns, which resulted in a significant improvement in the trajectory solution. The estimated PCRB for the same car is shown in Figure 6. Further, the standard deviation of the estimated trajectory solution is also overlaid in the same figure. It is interesting to note that PCRBs, both for easting and northing coordinates, exhibit a significant increase in value every time the car is turning. Easting PCRB is ~ 5 cm when the car is moving on the straight trajectory and grows to ~ 12 cm in turns. The PCRB along northing axis is varying from ~ 7 cm to ~ 11 cm when the car is driving on the straight trajectory and grows up to ~ 38 cm at turns. It is to be noted that standard deviations of estimated trajectories are mostly equal or, a little bit over PCRB, which is expected since the PCRB represents the theoretically best achievable performance.

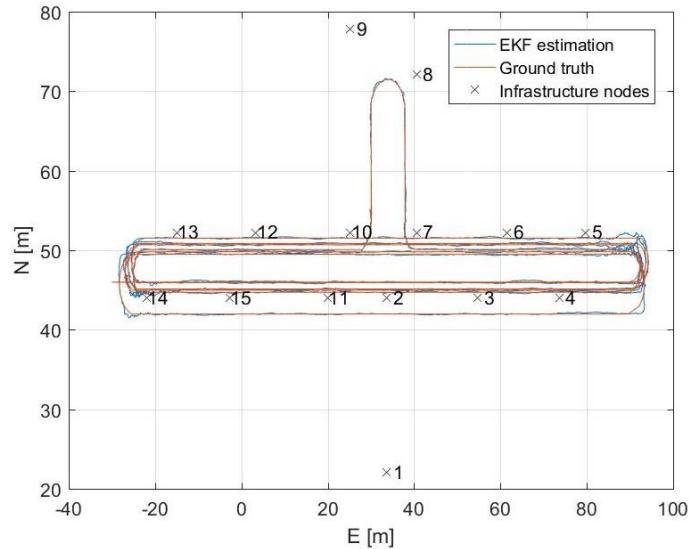


Figure 5. Position estimation for Car 1 in the network of 15 infrastructure nodes

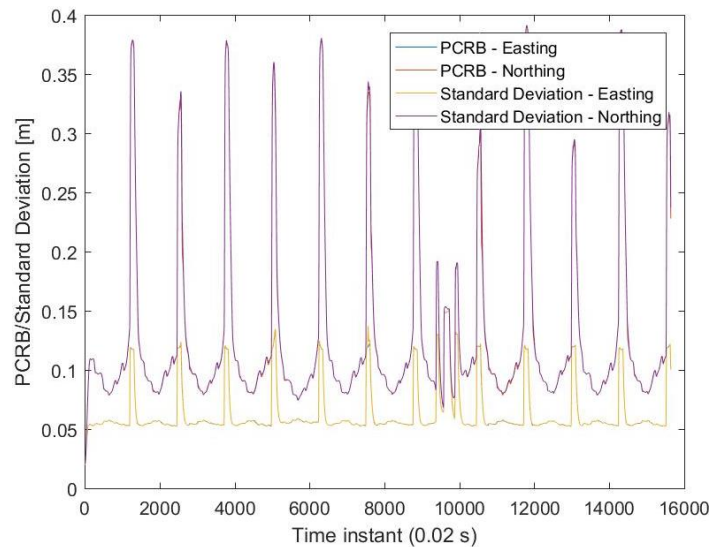


Figure 6. Dynamic PCRB for Car 1's position in the network of 15 infrastructure nodes

Performance accuracy of V-2-I positioning in the case of 15 infrastructure nodes is shown in Table 1. When looking at the trajectory as a whole, average 2D accuracy is 13.4 cm and 19.7 m for heights. However, the trajectory is divided into 3 main categories. The first one consists of straight parts of trajectory where the accuracy of position estimate is mostly around 10 cm in 2D and 20.5 cm in heights. The second category consists of all turns (except for the small loop) where the position is estimated with accuracies of 43.3 cm horizontally and 17.9 cm vertically. Position estimates in small SN (South-North) loop are on average around 24.6 cm horizontally and 5.9 cm vertically. Vertical accuracy is better than the horizontal accuracy because the cars are moving on an assumed horizontal plane at constant height of 100 m plus the added measurement noise.

15 nodes	Whole trajectory		Straight		Turns		Small SN loop	
	Hz [m]	h [m]	Hz [m]	h [m]	Hz [m]	h [m]	Hz [m]	h [m]
Average	0.134	0.197	0.100	0.205	0.433	0.179	0.246	0.059
Max	2.539	2.218	1.043	1.497	2.539	2.218	1.654	1.486
St. Dev.	0.177	0.241	0.089	0.237	0.392	0.278	0.222	0.183

Table 1. Accuracy of V-2-I in horizontal and vertical sense for network of 15 infrastructure nodes

In the second experiment, a network of 6 infrastructure nodes was used for V-2-I CP of Car 1. The geometry of those nodes is shown in Figure 7. The chosen geometry can be characterised as good because the PCRB does not show a significant increase in values with significant decrease in number of infrastructure nodes (i.e. from 15 to 6). Values of PCRB along the easting and northing axis have increased for ~3 cm when the car is moving on a straight part of trajectory, and ~5 to ~6 cm in turns (Figure 8). Table 2 shows a slight decrease in accuracy (from ~4 to ~9 cm horizontally and ~10 to ~15 cm vertically).

6 nodes	Whole trajectory		Straight		Turns		Small SN loop	
	Hz [m]	h [m]	Hz [m]	h [m]	Hz [m]	h [m]	Hz [m]	h [m]
Average	0.176	0.339	0.137	0.358	0.504	0.282	0.334	0.020
Max	2.528	1.707	1.083	1.707	2.528	1.264	1.689	0.099
St. Dev.	0.201	0.390	0.116	0.401	0.416	0.268	0.248	0.021

Table 2. Accuracy of V-2-I in horizontal and vertical sense for network of 6 infrastructure nodes

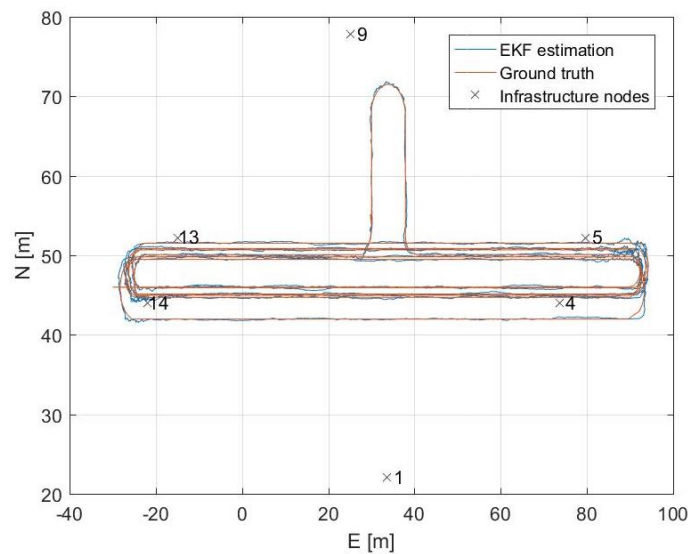


Figure 7. Position estimation for Car 1 in the network of 6 infrastructure nodes

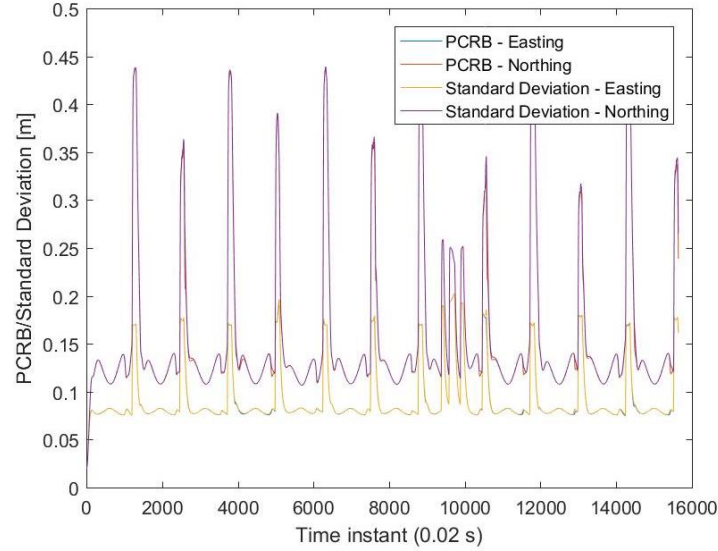


Figure 8. Dynamic PCRb for Car 1's position in the network of 6 infrastructure nodes

In the third experiment, a network of 4 infrastructure nodes (Figure 9) for CP is defined. In this network, separation distance between infrastructure nodes is greater in the east-west direction (~ 100 m) than in south-north direction (~ 10 m). The impact of such infrastructure node geometry on position estimation is visible in Figure 9, and in the PCRb graph in figure 10. It can be seen that the northing PCRb values have almost been doubled in comparison to the PCRbs in case of 15 and 6 infrastructure nodes. A slight increase in easting PCRb is shown, as well. The accuracy of the estimated trajectory has been significantly decreased (approximately 16 cm to 24 cm in both horizontal and vertical sense), which can be seen in Table 3.

4 nodes	Whole trajectory		Straight		Turns		Small SN loop	
	Hz [m]	h [m]	Hz [m]	h [m]	Hz [m]	h [m]	Hz [m]	h [m]
Average	0.313	0.382	0.273	0.394	0.649	0.340	0.488	0.196
Max	2.661	1.638	1.701	1.638	2.661	1.341	1.778	0.402
St. Dev.	0.269	0.385	0.204	0.399	0.480	0.288	0.318	0.058

Table 3. Accuracy of V-2-I in horizontal and vertical sense for network of 4 infrastructure nodes

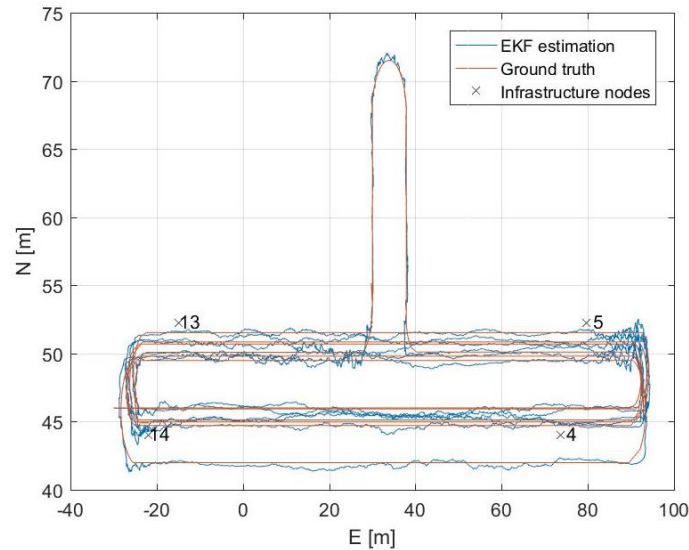


Figure 9. Position estimation for Car 1 in the network of 4 infrastructure nodes

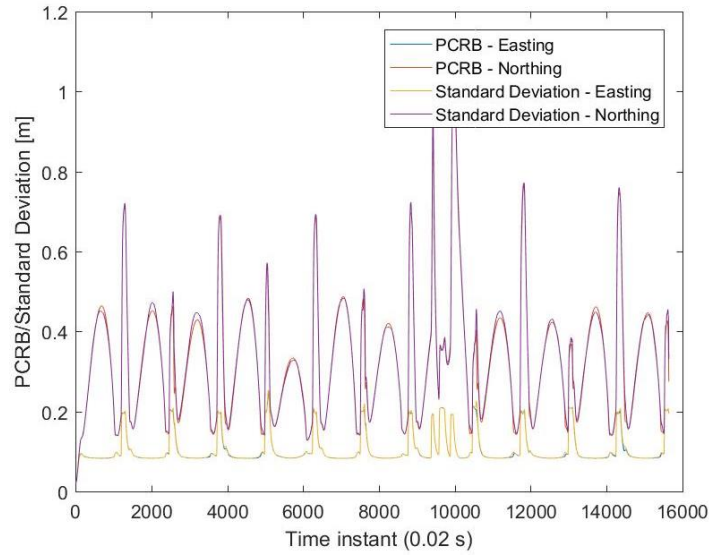


Figure 10. Dynamic PCRb for Car 1's position in the network of 4 infrastructure nodes

For the fourth experiment, the number of infrastructure nodes has been decreased further. Now, a network of 3 infrastructure nodes is proposed where nodes form a triangle (Figure 11). Even though the number of infrastructure nodes was decreased, the geometry has proven to be more important because of the better results in this experiment in the comparison to the previous one. Better results can be seen in Figure 12, as well. It can be seen that northing PCRb for the straight parts of the trajectory is lower for ~20 cm and ~10 cm for turns. Improvement of ~4 to ~6 cm can be seen in Table 4 as well.

3 nodes	Whole trajectory		Straight		Turns		Small SN loop	
	Hz [m]	h [m]	Hz [m]	h [m]	Hz [m]	h [m]	Hz [m]	h [m]
Average	0.244	0.348	0.200	0.349	0.612	0.483	0.426	0.021
Max	2.613	2.308	1.477	2.183	2.613	2.308	1.597	0.074
St. Dev.	0.242	0.436	0.159	0.418	0.470	0.602	0.279	0.017

Table 4. Accuracy of V-2-I in horizontal and vertical sense for network of 3 infrastructure nodes

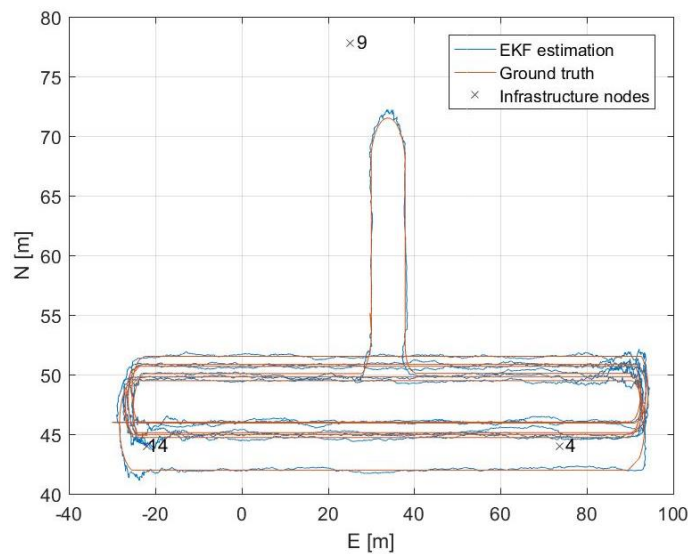


Figure 11. Position estimation for Car 1 in the network of 3 infrastructure nodes

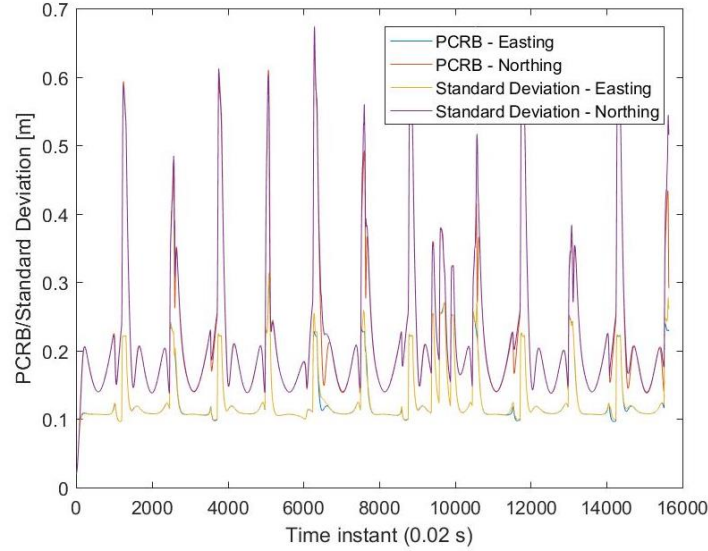


Figure 12. Dynamic PCRB for Car 1's position in the network of 3 infrastructure nodes

Presented results show that geometry of infrastructure nodes can deteriorate overall system's performance significantly. Since roads have linear geometry and ITS infrastructure must follow the roads, geometry of infrastructure nodes will follow the linear geometry of roads. As shown in the third experiment in this section, that linear geometry reduces system's performance.

5.2 Vehicle to Vehicle Cooperative Positioning

In this experiment, Car 1 estimates its own position based on the relative range measurements to all other cars and their GNSS positions (V-2-V). The measurements from static infrastructure nodes are not used in this analysis. As before, the mathematical model presented in Section 3 can be adapted for this case simply by excluding ranges measured to infrastructure nodes in the measurement vector Z_{k+1} , and by adapting joint measurement matrix H_{k+1} .

V-2-V CP simulation does not show good results. Firstly, in a system like this, where only GNSS of 3 other cars and relative ranges are available, there is a lack of measurements. Secondly, a solution highly depends on the relative geometry of all cars. Since only 4 cars were considered in this paper and the simulated road is 10.5 m wide, a good geometry could almost never be achieved, therefore a study on different geometries and their effects could not be performed. However, position estimation for the small loop seems to be good which is not surprising (Figure 13). The reason behind this is probably because the geometry becomes better when the Car 1 is driving through the small loop (i.e. Car 1 forms a triangle with other cars). Figure 14 shows the accuracy plot for the estimated trajectory of Car 1. Certain peaks in the accuracy graph of the northing coordinate can be noticed. Those are the peaks corresponding to the peaks of estimated trajectory in Figure 13, where the accuracy is at its lowest. The geometry of cars in those two moments is shown in Figure 15 and Figure 16. Both figures show similar geometry where all cars with GNSS are positioned on one side of the Car 1 at distances bigger than ~35m. This geometry is inadequate, especially when a 10.5 m wide road is in question and the car is starting to change the direction of driving.

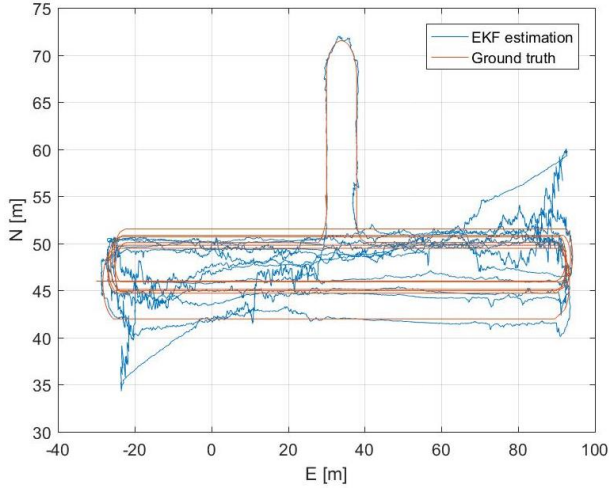


Figure 13. Position estimation of Car 1 for V-2-V CP

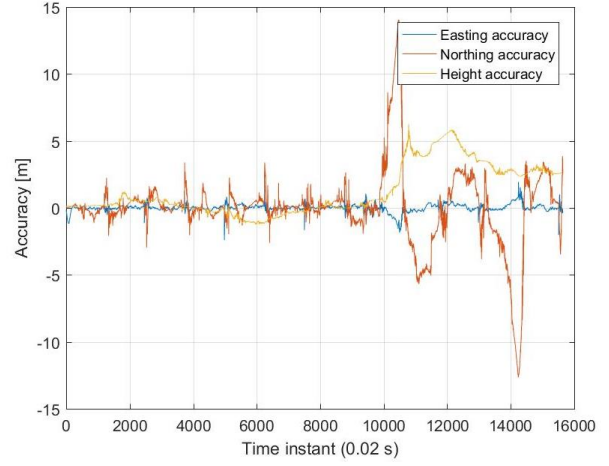


Figure 14. Position accuracy of Car 1 for V-2-V CP

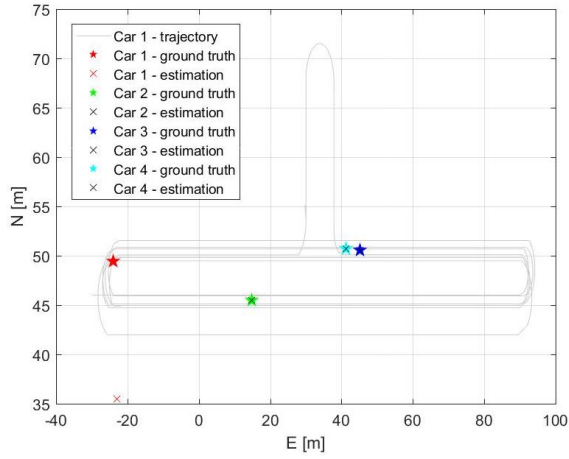


Figure 15. The geometry of the cars in the time instant 10480

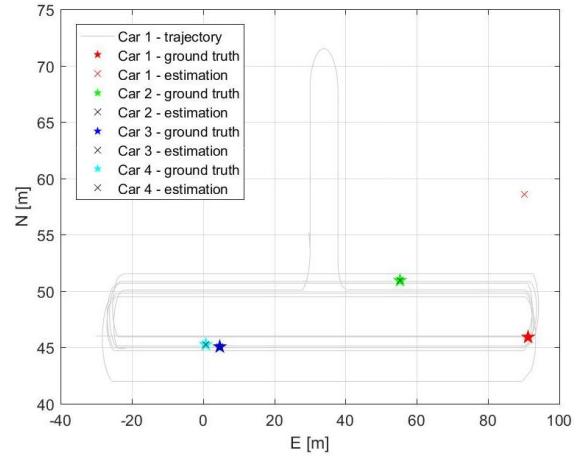


Figure 16. The geometry of the cars in the time instant 11110.

5.3 Vehicle to Infrastructure and Vehicle to Vehicle Cooperative Positioning

Lastly, combined V-2-I and V-2-V CP performance is presented. In these experiments, it is assumed that Car 1 measures ranges to all the other cars and infrastructure nodes, and receives GNSS positions from other cars. Because it is combined solution, a slight increase in accuracy should be expected.

Figure 17 shows the trajectory estimation of the Car 1 in the system described above. Calculated PCRBs are presented in Figure 18, and are very similar in values to the PCRBs of the V-2-I performance for the network of 15 infrastructure nodes (Figure 5). Table 5 provides information about CP performance accuracy. Although 2D estimation accuracy goes down to 2.5 m in turns, the overall accuracy of the system is promising for further development. Furthermore, a slight improvement in 2D accuracy in comparison to the 2D accuracy of the matching V-2-I solution (Table 1) is visible. Although the improvement is minor (from 0.3 cm to 1.4 cm), it shows the potential in using the combined system. Furthermore, in this case, because so many infrastructure nodes are available in comparison to the number of cars, it can be seen that poor geometry of the cars does not have an impact on the final positioning solution shown in Figure 17.

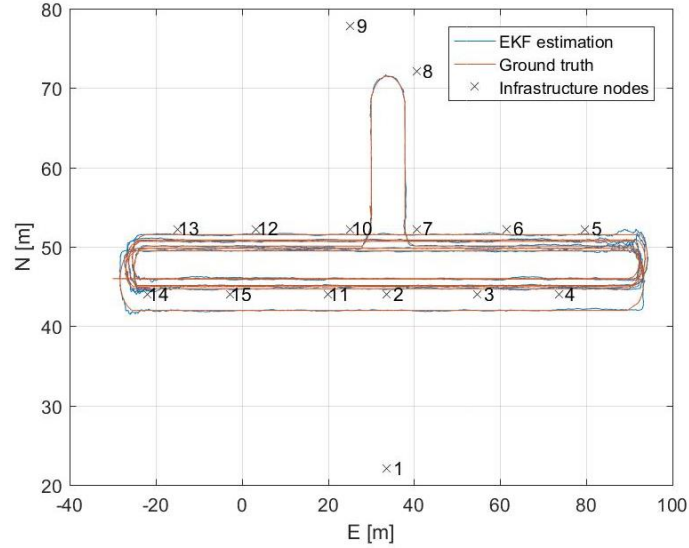


Figure 17. Position estimation of Car 1 for V-2-V+V-2-I solution

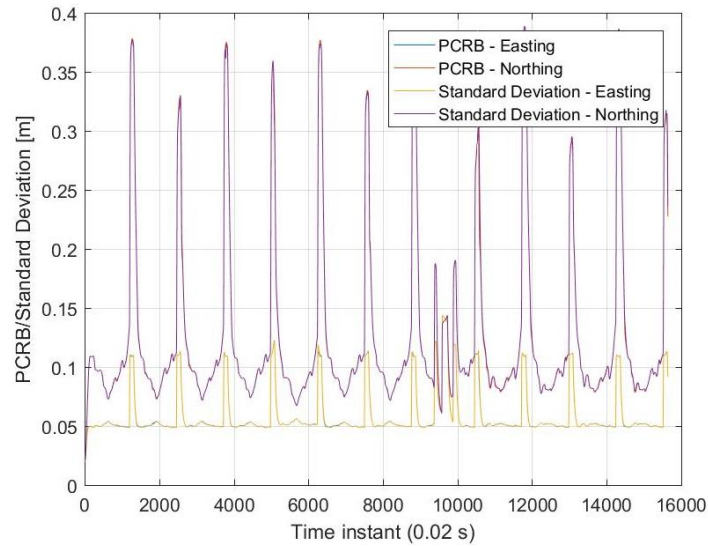


Figure 18. Dynamic PCRb for Car 1's position for V-2-V+V-2-I solution

	Whole trajectory		Straight		Turns		Small SN loop	
	Hz [m]	h [m]	Hz [m]	h [m]	Hz [m]	h [m]	Hz [m]	h [m]
Average	0.131	0.201	0.098	0.208	0.425	0.197	0.232	0.040
Max	2.508	1.667	1.040	1.667	2.508	1.552	1.650	0.611
St. Dev.	0.175	0.228	0.088	0.225	0.388	0.275	0.222	0.070

Table 5. Accuracy of V-2-I + V-2-V positioning in horizontal and vertical sense

6. CONCLUSION AND FUTURE WORK

The best theoretical performance achievable for the proposed CP system is determined using PCRb analysis and is less than 40 cm when a car is turning, and ~10 cm when the car is driving on a straight line. Achieving this accuracy offers significant benefits for almost every ITS application. Therefore, it can be concluded that these results are a promising start to developing a CP framework appropriate for road applications. One of the major vulnerabilities of CP for land vehicles is the geometry of the infrastructure nodes, as well as the mobile nodes. As

represented in this paper, CP is constrained by the very shape of the roads. Given the dynamic and complex geometry of the mobile nodes in a vehicular network, the results indicate that fixed network of infrastructure nodes would assist in constraining the accuracy of the solution.

In the future, integrating IMU data with GNSS and relative ranges needs to be done because IMU has the potential of addressing problems of lack of measurements in proposed ad hoc network in V-2-V cooperative positioning. Furthermore, having IMU data available would make the proposed framework more appropriate for urban environments where more than one car can be without GNSS measurements. This would assure that even in the absence of GNSS data for multiple cars, relative ranges would not be the only basis of calculating the estimated positions. The future work is aimed at experimental validation and evaluation of the framework presented in this paper.

REFERENCES

- Alam N, Dempster AG (2013), Cooperative positioning for vehicular networks: facts and future, *IEEE Transactions on Intelligent Transportation Systems*, Vol. 14, No. 4: 1708-1717.
- Gholami MR, Gezici S, Ström EG (2012), Improved position estimation using hybrid TW-TOA and TDOA in cooperative networks, *IEEE Transactions on Signal Processing*, Vol. 60, No. 7: 3770-3785.
- Goel S (2017) A distributed cooperative UAV swarm localization system: Development and analysis, *Proceedings of the 30th International Technical Meeting of The Satellite Division of the Institute of Navigation (ION GNSS+ 2017)*, Portland, Oregon, September 25-29, 2017, pp. 2501-2518.
- Goel S, Kealy A, Gikas V, Retscher G, Toth C, Brzezinska DG, Lohani B (2017), Cooperative localization of Unmanned Aerial Vehicles using GNSS, MEMS Inertial and UWB sensors, *Journal of Surveying Engineering*, 143(4), doi: 10.1061/(ASCE)SU.1943-5428.0000230.
- Goel S, Kealy A, Lohani B (2016), Cooperative UAS localization using low cost sensors, *ISPRS Annals of Photogrammetry Remote Sensing and Spatial Information Science*, ISPRS Congress, Prague, Czech Republic, III-1:183-190.
- Larsson EG (2004), Cramér–Rao Bound analysis of distributed positioning in sensor networks, *IEEE Signal Processing Letters*, Vol. 11, No. 3: 334-337.
- Penna F, Caceres MA, Wymeersch H (2010), Cramér–Rao Bound for hybrid GNSS-terrestrial cooperative positioning, *IEEE Communications Letters*, Vol. 14, No. 11: 1005-1007.
- Popescu DC, Hedley M, Sathyan T (2013) Posterior Cramér–Rao Bound for anchorless tracking, *IEEE Signal Processing Letters*, Vol. 20, No. 12: 1183-1186.
- Shladover SE, Tan SK (2006), Analysis of vehicle positioning accuracy requirements for communication-based cooperative collision warning, *Journal of Intelligent Transportation Systems: Technology, Planning, and Operations*, 10:3: 131-140.
- Taylor JH (1979) The Cramér–Rao estimation error lower bound computation for deterministic nonlinear systems, *IEEE Transactions on Automatic Control*, Vol. AC-24, No. 2: 343-344.
- Yao J, Balaei AT, Hassan M, Alam N, Dempster A (2011), Improving cooperative positioning for vehicular networks, *IEEE Transactions on Vehicular Technology*, Vol. 60, No. 6: 2810-2823.